Li_4MgReO_6: An $S=1/2$ antiferromagnet exhibiting spin-glass behavior

M. Bieringer and J. E. Greedan
Brockhouse Institute for Materials Research and Department of Chemistry, McMaster University, Hamilton, Ontario, Canada L8S 4M1

G. M. Luke
Brockhouse Institute for Materials Research and Department of Physics and Astronomy, McMaster University, Hamilton, Ontario, Canada L8S 4M1

(Received 2 September 1999)

Polycrystalline Li_4MgReO_6 was prepared by means of solid-state synthesis. The crystallographic structure was determined from high-resolution powder-neutron-diffraction data. It was found that Li_4MgReO_6 crystallizes in space group $C2/m$ with lattice parameters, $a=5.0978(3)$ Å, $b=8.8163(5)$ Å, $c=5.0815(3)$ Å, and $\beta=109.835(2)°$. This structure is an ordered variant of Li_2SnO_3 in which Li^+, Mg^{2+}, and Re^{6+} ions occupy the Sn^{4+} sites, which can be desribed as honeycomb layers. Due to the large differences in formal charge, the Re^{6+} ions order on half of the Sn sites forming a distorted face-shared tetrahedral sublattice. As Re^{6+} is an $S=1/2$ ion this material is an attractive candidate for the study of the effects of geometric frustration on a quantum spin system. The investigation of bulk magnetic susceptibilities and magnetization studies as well as low-temperature neutron-diffraction experiments reveals a spin-glass behavior with a glass transition temperature of 12 K. Both heat-capacity and muon spin-relaxation measurements at low temperatures are consistent with a spin-glass interpretation with no long-range order detectable down to $T=0.5$ K.

I. INTRODUCTION

Extensive investigations of triangular antiferromagnets have been carried out during the last two decades. The fact that not all three antiferromagnetic exchange constraints can be satisfied simultaneously creates a frustrated situation, which is illustrated in Fig. 1. In the past, different magnetic ground states were proposed for triangularly frustrated lattices. Most such compounds show a Neél ground state, which can be established if all spins are oriented at an angle of 120° with respect to each other (see Fig. 1 also). The resulting net magnetic moment is zero and the structure is chiral. On an ideal triangular lattice each of the chiral configurations can form a continuum of degenerate ground states if all magnetic moments are rotated simultaneously in the x-y plane such that the 120° constraint is still satisfied. Examples of triangular antiferromagnets are $LnMnO_3$ (Ln $=$Ho,Er,Tm,Lu),[1] $ScMnO_3$,[2] $CsMnBr_3$,[3,4] as well as VX_2 ($X=$Cl, Br, and J) and $ACrX_2$ ($A=$Li, Na, K, and $X=$O, S, Se).[5] In 1973 a new magnetic ground state was proposed by Anderson.[6] For the case of a $S=1/2$ system, Anderson suggested a model involving the formation of spin singlets, based on the pairing of adjacent spins, which satisfies the antiferromagnetic coupling condition. It is easy to imagine that there exists a large number of combinations of nearest-neighbor singlet pair formations. Consequently no magnetic long-range order is established, but a high degree of degeneracy is achieved upon application of linear combinations of individual spin configurations, which lowers the total energy. In analogy to the chemical bonding models of Pauling, this was called the resonating valence bond model. This also represents a spin-liquid type ground state, since no ''condensation'' into either a Neél state or a frozen spin or spin-glass state occurs. The different spin configurations of a spin liquid are separated by a zero-energy barrier. In 1974, Fazekas and Anderson[7] published a detailed analysis of the triangular lattice for $S=1/2$ spins. It has been pointed out that a high degree of anisotropy is favorable for the formation of the spin liquid type ground state.

Since 1974 several magnetic systems have been investigated experimentally, in a search for real spin liquids, including $LiNiO_2$,[8] $LiCoO_2$, $NaTiO_2$,[9] and $SrCr_4Ga_8O_{19}$ (Ref. 10) where interesting data concerning the spin dynamics at low temperatures were obtained. In the latter, the paramagnetic Cr^{3+} ions are located on a *kagomé* lattice (corner-shared triangular lattice) as well as in layers of edge-sharing triangles. Lately, the jarosite family has attracted attention, since this is the first example of a *kagomé* structure with no disorder present, thus representing an interesting model compound for spin-liquid behavior.[11]

Another interesting ground state, already mentioned, is the spin-glass state, where the magnetic moments freeze randomly upon cooling the sample below a characteristic temperature. It is noteworthy that short-range order might be present on the magnetic sublattices. Spin glasses were investigated extensively in the 1970's, in particular dilute metallic spin glasses were considered, whereas interest in spin glasses of magnetic insulators developed in the 1980's. For most cases site disorder on the magnetic sublattice is considered a necessary requirement for the formation of a spin-glass ground state. In the two broad classes positional disorder is a prominent feature as the concentration of the magnetic ion on its sublattice is below the appropriate percolation limit. There does exist a small class of insulating magnetic materials in which the magnetic sublattice appears to be fully occupied, i.e., with defect levels at or near the limit of detection by diffraction methods, and thus, with concentration levels well above any percolation threshold, which nonetheless exhibit spin-glasslike behavior. In such materials the

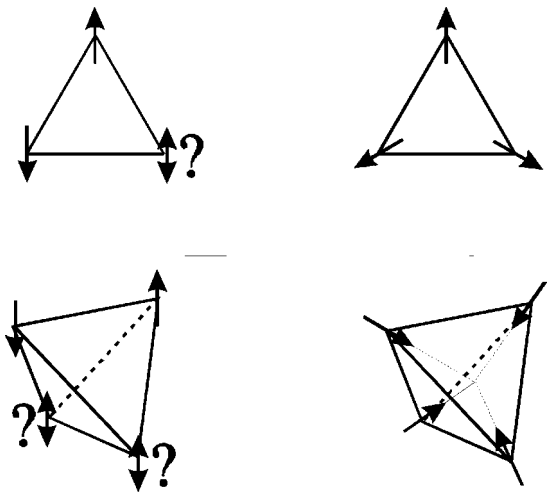

FIG. 1. Illustration of a magnetically frustrated triangular lattice (upper figure) with antiferromagnetic coupling constant J_1. Only two spins can be aligned antiparallel, whereas the third spin is frustrated. The lower figure shows the geometrically frustrated situation on the four vortices of a tetrahedron.

magnetic sublattice is geometrically frustrated and the nearest-neighbor exchange spin coupling is antiferromagnetic. An example is the pyrochlore oxide $Y_2Mo_2O_7$.[12]

Many of the candidate spin-liquid materials mentioned above crystallize in an ordered variant of the NaCl structure, with a 1:1 ratio of magnetic to nonmagnetic ions, e.g., $LiNiO_2$, $LiCoO_2$, and $NaTiO_2$. In these cases, order on the cation sublattice results in a geometrically frustrated magnetic sublattice with layers of edge-sharing equilateral triangles. It is of interest to investigate other ordered NaCl structures with different magnetic to nonmagnetic ion ratios. One such example is the α-Li_2SnO_3 structure type. In this case the Sn^{4+} sublattice consists of layers with a honeycomb topology. Cation ordering on half of the sites in such a lattice would result in an edge-sharing triangular layer, as in Fig. 1, or a tetrahedral sublattice depending on the layer spacing. The problem, then, is to find a combination of ions which are likely to exhibit charge ordering and one of which is an $S=1/2$ ion. A solution to the problem may be the material Li_4MgReO_6 in which Re^{6+} [$5d$ (Ref. 1, $S=1/2$] is paired with Mg^{2+}. This compound was first reported in 1963 along with Li_5ReO_6, which is apparently isostructural, but a detailed crystal structure of Li_4MgReO_6 was not presented.[13] Somewhat later Lang[14] considered the symmetry of different stacking sequences of the Re^{6+} containing layers and suggested monoclinic $C2/m$ and $C2/c$ and trigonal space groups, $P3_112$ and $P3_212$, but again no detailed structure. The availability of only x-ray powder samples has been an impediment to a structure solution. An additional issue with a Re^{6+} material is whether the d electron will remain localized. ReO_3 is well-known to be metallic, but the ordered perovskite Sr_2MgReO_6 is insulating.[15] Given the level of dilution of Re^{6+} in the proposed cation-ordered structure one would expect Li_4MgReO_6 to be insulating and magnetic as well.

In this paper we present the preparation of polycrystalline Li_4MgReO_6, and the crystallographic structure of Li_4MgReO_6 as derived from powder-neutron-diffraction data. Of central interest is the geometry of the Re^{6+} sublattice and the significance of the disorder of magnetic as well as nonmagnetic ions in the structure.

The results of a detailed study of the magnetic properties including bulk magnetic susceptibility and time-dependent relaxation experiments are presented. The observations are supplemented by heat-capacity, low-temperature neutron-diffraction, and muon spin-relaxation experiments that are crucial in the characterization of the magnetic ground state.

II. EXPERIMENT

A. Preparation of polycrystalline Li_4MgReO_6

Li_2O was prepared at 650 °C under vacuum from LiOH H_2O ($\geqslant$99.9% Smith Chemicals) according to the following reaction:

$$2\ \mathrm{LiOH}\ \ \mathrm{H_2O} \rightarrow \mathrm{Li_2O} + 3\mathrm{H_2O}. \tag{2.1}$$

Li_4MgReO_6 was prepared from Li_2O, MgO (Cerac, 99.99%), Re_2O_7 (Cerac, 99.9%), and Re (Cerac, 99.99%). Stochiometric amounts of the starting materials were ground and placed in a Pt crucible, which was placed in a sealed and evacuated quartz tube. The synthesis was carried out for 24 h at 650 °C according to reaction (2.2).

$$2\ \mathrm{Li_2O} + \mathrm{MgO} + \frac{3}{7}\mathrm{Re_2O_7} + \frac{1}{7}\mathrm{Re} \rightarrow \mathrm{Li_4MgReO_6}. \tag{2.2}$$

All preparative steps were carried out in a glove box (Ar atmosphere). After completion of the reaction a very small amount of white deposit (Li_2O or MgO) was found on the walls of the quartz tube. The polycrystalline product is black and homogeneous. A two probe resistance measurement indicated insulating behavior.

B. X-ray powder diffraction

The product purity was determined with a focussing Guinier Hägg camera using $Cu_{K\alpha}$, x-ray radiation, $\lambda = 1.54060$ Å. Accurate unit-cell constants were obtained and no impurities were identified.

C. Neutron powder diffraction

1. Room temperature neutron-powder-diffraction experiments

Time of flight neutron-powder-diffraction experiments were carried out at IPNS at Argonne National Laboratory on instrument SEPD using a vanadium sample can, spanning the d-spacing range 0.4 Å–4 Å.

2. Low-temperature neutron-powder-diffraction experiments

Neutron-powder-diffraction experiments at low temperatures were carried out on the C2 diffractometer (800 wire position sensitive detector) operated by the Neutron Program for Materials Research of the National Research Council of Canada at the Chalk River Nuclear Laboratory using a wavelength $\lambda = 1.32632$ Å. Powder-diffraction patterns were taken in a vanadium sample can over the 2θ range 3°–83°. In order to investigate potential magnetic long-range order, experiments were carried out at 4 K, 20 K, and 40 K using helium cryostat H8.

D. Magnetic susceptibility measurements

Bulk magnetic measurements were carried out using a superconducting quantum interference device (SQUID), magnetometer (Quantum design). Using magnetic fields of 0.1 and 1 T, magnetic susceptibilities were obtained between 2 K and 500 K. Between 2 K and 350 K the measurements were carried out in gelatin capsules within the He cryostat. The data for the high-temperature region between 300 K and 500 K were collected using a quartz tube within an oven. Furthermore, magnetization curves were taken at 5 K, 10 K, and 15 K, where the magnetic field was swept from 0 to 5.5 T.

E. Magnetic relaxation measurements

Magnetic relaxation measurements were carried out at 5 K, 10 K, and 20 K using a SQUID magnetometer (Quantum Design). The sample was cooled to 5 K in zero field. As soon as $T=5$ K was reached a magnetic field of $H=0.1$ T was switched on and the magnetization was monitored as a function of time. Before measuring the next temperature the sample was warmed to $T=50$ K in order to be far above the glass transition temperature of 12 K.

F. Heat-capacity measurements at low temperatures

The specific heat in zero field of the sample in the form of a pellet was measured in the temperature range 0.6–30 K using a quasiadiabatic calorimeter and a commercial Heliox sorption pumped ^{3}He cryostat. The pulse method was used for these measurements. The sample was mounted on a thin sapphire plate with apiezon for better thermal contact. Underneath the sapphire plate a strain gauge heater and a RuO_2 temperature sensor were attached. The specific heat of the sample was obtained by subtracting the contribution of the addendum, measured separately, from the total measured heat capacity.

G. Muon spin relaxation measurements

Muon spin relaxation measurements were carried out at TRIUMF in Vancouver. The zero-field experiments covered the temperature range 2.5 K–125 K. Furthermore, longitudinal field experiments using applied magnetic fields of 0.01 T and 0.1 T were carried out.

III. RESULTS AND DISCUSSION

A. Diffraction experiments

X-ray powder patterns were collected using a Guinier Hägg camera where Si was used as an internal standard. Using the unit cell search routine VISSER (version 9) a monoclinic unit cell with space group $C2/m$ was found for 20 reflections. The unit-cell dimensions were refined using the least-square minimization program LSUDF. Forty-one reflections were used for the refinement resulting in the following unit-cell constants: $a=5.0941(3)$ Å, $b=8.809(2)$ Å, $c=5.0801(8)$ Å, and $\beta=109.875(1)°$. The unit cell as well as the space group found for Li_4MgReO_6 agrees with Li_5ReO_6.[16] However, earlier work on Li_4MgReO_6 (Ref. 14) suggested three different possible unit cells based on the space groups $C2/m$, $C2/c$ as well as $P3_112$ and $P3_212$. Only $C2/m$ accounted for all reflections. This result was confirmed with neutron-powder-diffraction data as well.

TABLE I. Agreement factors and refined lattice parameters for Li_4MgReO_6 as determined from Rietveld refinement of powder-neutron-diffraction data at room temperature.

Number of data points	5299	a [Å]	5.0979(3)
Number of parameters	32	b [Å]	8.8163(5)
R_{wp}	5.53	c [Å]	5.0815(3)
R_p	3.66	β [°]	109.835(2)
Reduced χ^2	1.86	V [Å^3]	214.83(2)
Space group	$C2/m$		

B. Crystallographic structure of Li_4MgReO_6

1. Refinement of Li_4MgReO_6 from powder-diffraction data

The crystallographic structure of Li_4MgReO_6 at room temperature was determined from time of flight neutron-powder-diffraction data obtained at Argonne National Laboratory on instrument SEPD. 5299 observed data points were used and 32 parameters refined. The refinements were carried out sequentially such that the occupancies were refined at an intermediate stage but held constant during the final cycle. Using the refinement package GSAS (Ref. 17) the 32 parameters included atomic positions, temperature factors, occupation factors, background parameters, cell constants, the absorption coefficient, and preferred orientation parameters. The unit-cell parameters determined from the neutron-powder-diffraction data are reasonably close to the values found with the Guinier camera, the unit-cell dimensions and the agreement factors for the Rietveld refinement are reported in Table I. Figure 2 shows the Rietveld refinement of the neutron-powder pattern obtained at room temperature.

$$R_{wp}=100\sqrt{\frac{\sum_i w_i[y_i-y_{ic}]^2}{\sum_i w_i y_i^2}} \tag{3.1}$$

$$R_p=100\frac{\sum_i |y_i-y_{ic}|}{\sum_i |y_i|} \tag{3.2}$$

The occupancies were refined such that all sites are fully occupied and that the Li^+ and Mg^{2+} ratio was refined as well. All possible combinations of cation mixing on the cation sites were tested. The Re^{6+} site did not allow any substitution by Li^+ or Mg^{2+}, therefore in the final refinement cycles for the occupation factors no Li and Mg was allowed on the Re site. The structural parameters obtained from Rietveld analysis of time of flight neutron-powder data are presented in Table II.

The stochiometry derived from the occupation factors is $Li_{3.96}Mg_{1.04}ReO_6$, which is in reasonable agreement with the nominal composition of Li_4MgReO_6. The crystallographic structure of Li_4MgReO_6 is shown in Fig. 3 and is isostructural with Li_5ReO_6, which was determined from single-

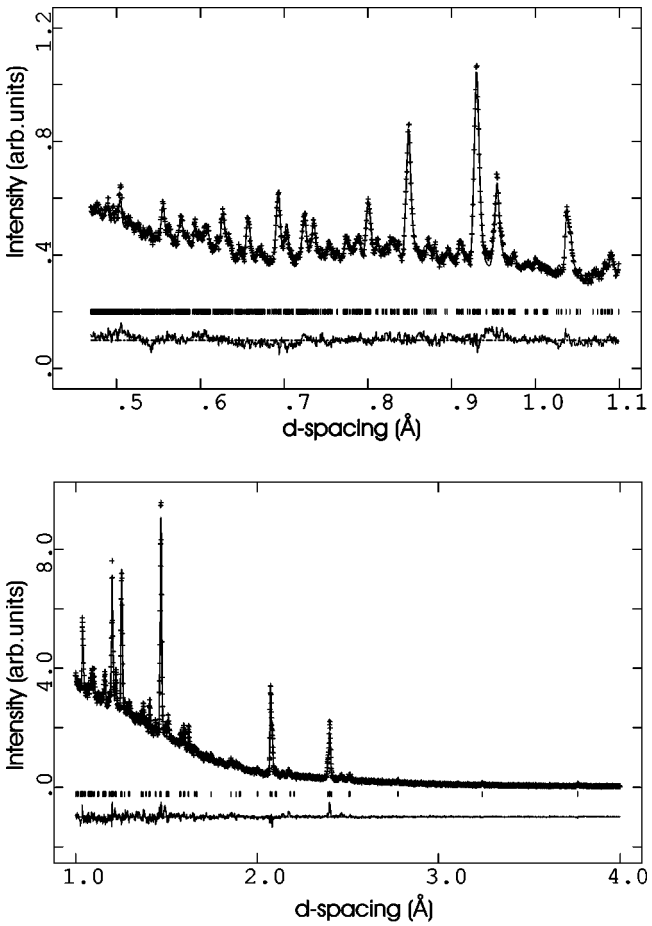

FIG. 2. Room temperature time of flight powder-neutron-diffraction pattern obtained at IPNS.

crystal x-ray data.[16] Both structures are based on α-Li_2SnO_3. All cations are in slightly distorted octahedral environments. The cation-oxygen octahedra are edge shared, consequently the structure is well described as an ordered rock salt structure. The cation distribution can be described in terms of layers, which are stacked perpendicular to the *ab* plane. The first layer contains Li^+ and Mg^{2+} ions only. Every other layer accommodates Li^+, Mg^{2+}, and Re^{6+} ions. Therefore, in terms of stacking, the Re^{6+} ion containing layers are separated by Li^+, Mg^{2+} containing sheets, see Fig. 3. Lang described the structure as a two-dimensional honeycomb structure.[14] However, the shortest Re-Re distance is found

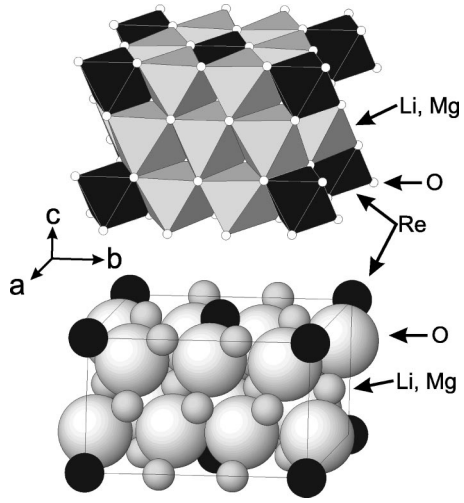

FIG. 3. The crystal structure of Li_4MgReO_6 can be described as an ordered NaCl structure having a monoclinic unit cell.

along the stacking direction, e.g., the crystallographic *c* axis. Since the Re-Re distances in the *ab* plane are only slightly larger than along the stacking direction, the Re^{6+} network is better described as a three-dimensional sublattice. The Li^+, Mg^{2+} cations are randomly disordered on their sites with a Li^+ to Mg^{2+} ratio close to 4:1 as required by the stochiometry, see Table II, whereas, the Re^{6+} site does not show any disorder. The separation of the (Li^+,Mg^{2+}) sublattice from the Re sublattice can be rationalized in terms of charge ordering. The high charges on the Re^{6+} ions can be accommodated best in the structure by permitting only mono- and divalent cations in the vicinity of Re^{6+}, thus excluding Re^{6+} from these sites. The main focus of this paper is the magnetism associated with the Re^{6+} sublattice, therefore it is particularly important to look at the topology of that sublattice. The Re^{6+} ions form tetrahedra with edge lengths between 5.08 Å and 6.55 Å. These distorted tetrahedra share faces throughout the structure, thus presenting a highly frustrated situation for antiparallel alignment of spins. The Re^{6+} sublattice is presented in Fig. 4, one tetrahedral face is shaded in order to emphasize the connectivity of the Re^{6+} tetrahedra by faces. The triangular faces in the *ab* plane are nearly equilateral with angles of 59.962° and 60.075°. The tetrahedra are more distorted in the *c* axis stacking direction giving triangular face angles of 54.787°, 70.165°, and 55.048°.

TABLE II. Li_4MgReO_6 structural data from the Rietveld refinement for space group $C2/m$.

Atom	*x*	*y*	*z*	U_i/U_e100	Occupancy
Li(1)	0	0.666(4)	0	6.4(7)	0.74(2)
Mg(1)	0	0.666(4)	0	6.4(7)	0.26(2)
Li(2)	1/2	0.315(5)	1/2	6.4(7)	0.84(2)
Mg(2)	1/2	0.315(5)	1/2	6.4(7)	0.16(2)
Li(3)	0	1/2	1/2	6.4(7)	0.80(2)
Mg(3)	0	1/2	1/2	6.4(7)	0.20(2)
Re(4)	0	0	0	1.01(6)	1.0000
O(5)	0.2598(7)	0.3445(3)	0.7603(5)	0.78(5)	1.0000
O(6)	0.2658(9)	1/2	0.2297(8)	1.12(8)	1.0000

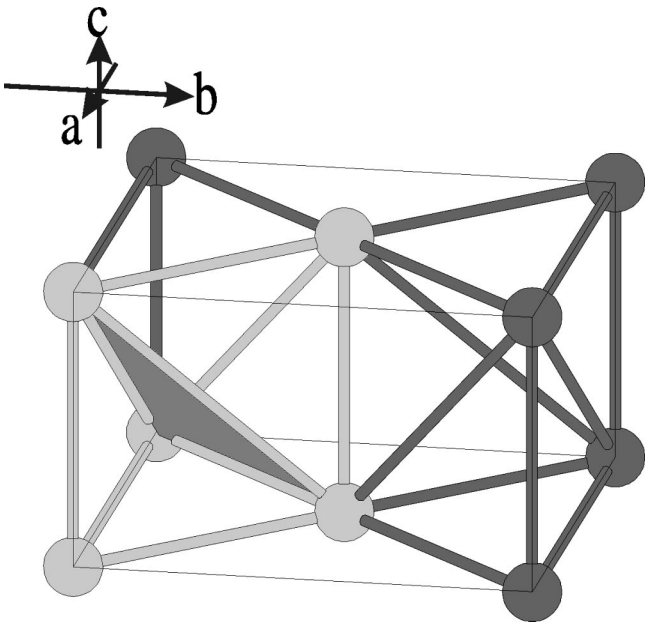

FIG. 4. Re^{6+} sublattice in Li_4MgReO_6. The Re cations form a highly frustrated three-dimensional sublattice consisting of face sharing tetrahedra.

2. Potential magnetic exchange paths for Re-Re interactions

There are five different Re-Re distances for each Re^{6+} tetrahedron 5.0815(3) Å (001), 5.0978(3) Å (100), 5.0920(6) Å (220), 5.8506(3) Å (101), and 6.5546(3) Å (221). The tetrahedral Re framework is indicated in Fig. 4 and the distances are shown in Fig. 5. The formal exchange path consists of a Re-O-(Li, Mg)-O-Re link. Due to the fact that all cations are octahedrally coordinated and all octahedra are sharing edges, there exist two basic types of exchange pathways. First, there are six similar Re-O-(Li, Mg)-O-Re links between two Re ions. Due to the distortion of the octahedra these six paths are not equivalent, but are very similar. Alternatively the exchange could occur via Re-O-O-Re, where there are three different possible paths between neighboring Re ions in the *ab* layers. However, the O-O distances

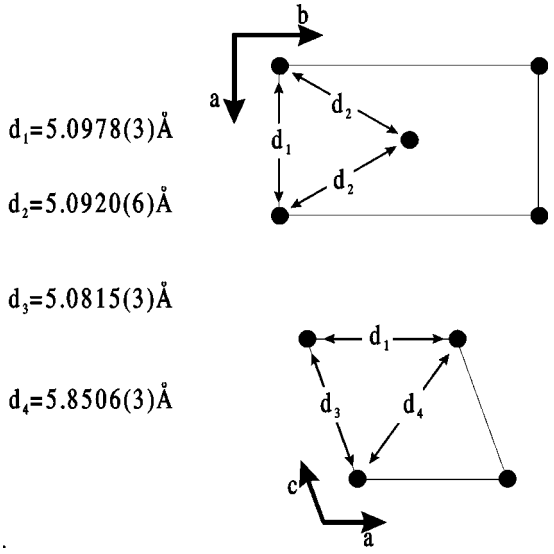

FIG. 5. Re-Re distances in Li_4MgReO_6.

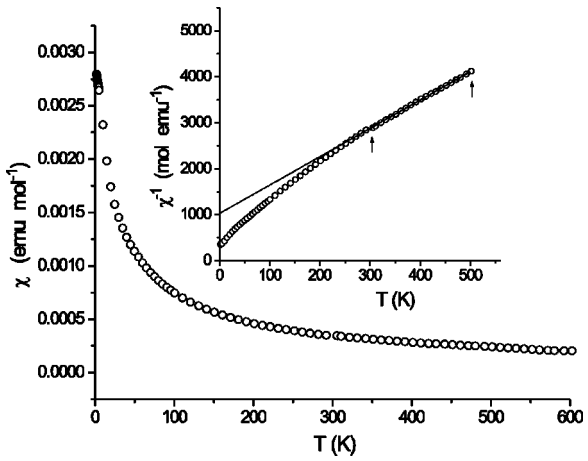

FIG. 6. Magnetic susceptibility measurements carried out using $H=1$ T. The inset shows the Curie-Weiss plot; the solid line is the best fit for $\chi=C/T-\theta$, the fitting range is indicated by the two upward pointing arrows.

are rather large (2.7–3.1 Å) and there is no reason to believe that there is any contact (overlap) between neighboring O^{2-} ions.

3. Bond disorder in Li_4MgReO_6

For the longest time, spin-glass behavior was considered to depend on disorder within the crystallographic lattice. The system presented here does not show any Re^{6+} disorder according to the Rietveld refinement carried out on the neutron-powder-diffraction data. However, the (Li, Mg) sites show disorder thus creating bond disorder, that means that the exchange paths and the orbital overlap depends on the local environment of each of the Re cations.

C. Magnetic susceptibility

Using magnetic fields of 0.1 T and 1 T the magnetic susceptibility of polycrystalline Li_4MgReO_6 was measured. No features indicating long-range order are present. However at low temperature, hysteresis behavior is found. The magnetic susceptibility data are presented in Figs. 6 and 7. The data do

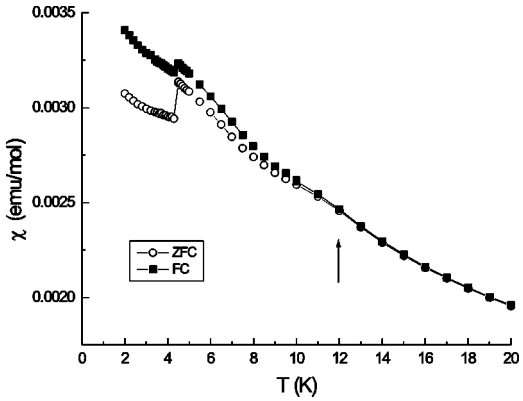

FIG. 7. Magnetic susceptibility measurements carried out at low temperatures using a magnetic field of $H=0.1$ T. The zero-field cooled and field cooled data diverge below 12 K. The step at 4.2 K is due to the instrumentation (refilling of the liquid He reservoir in the SQUID magnetometer).

not show the typical maximum in χ versus T for antiferromagnetic long-range ordering. Furthermore, the true Curie-Weiss region is not reached until about 350 K, the data for the temperature range 350 K to 500 K were fitted to the Curie-Weiss law,

$$\chi = \frac{C}{T-\theta}, \tag{3.3}$$

where C is the Curie constant and θ the Weiss temperature. The fit revealed $\theta = -166(3)$ K indicating strong antiferromagnetic coupling. The effective magnetic moment was determined to be $\mu_{eff} = 1.14(1)$BM, whereas the spin only value for Re^{6+} is 1.73BM. The low value of μ_{eff} may reflect admixture of an orbital component due to the rather large spin-orbit coupling expected for a $5d$ series ion. Using empirical psuedopotential method experiments the anisotropic g values for Re^{6+} in MoO_3-Re were determined to be very close to 1.6 and almost isotropic.[18] When we use $g = 1.6$ we find an expected effective magnetic moment of 1.39BM, which is much closer to the experimental value for Li_4MgReO_6. At low temperatures a divergence between zero field and field cooled magnetic susceptibilities is seen. The divergence sets in at 12 K. No indication of long-range magnetic ordering is present, both traces increase monotonically with decreasing temperatures, showing only changes in the slopes. No cusp, which is often found for spin-glasses, is present, however a cusp is not a necessary requirement for a spin-glass. At 4.2 K a step in the χ versus T curves is observed, which is caused by a delay during the measurement, which is due to the refilling of the He reservoir in the SQUID magnetometer. Therefore, the step is an experimental artifact but at the same time it emphasizes the time dependence of the magnetization. The inflection point at 12 K and the divergence below that temperature clearly indicate hysteresis, which supports the presence of possible cooperative magnetism. In order to investigate this, hysteresis relaxation measurements were carried out at 5 K, 10 K, and 20 K. The sample was cooled in the absence of a magnetic field and, after switching on a magnetic field of 0.1 T, magnetic susceptibility data were collected over a time of approximately 5 h. At 5 K and at 10 K a biexponential saturation behavior is observed, whereas at 20 K no saturation is seen. No attempt to explain the saturation behavior at 5 K and 10 K is undertaken, however, the absence of magnetic saturation at 20 K is in agreement with the proposed cooperative magnetism below 12 K. The dc-magnetic relaxation measurements are shown in Fig. 8. In addition, the magnetization versus magnetic-field strength data (Fig. 9) show a linear behavior for 5 K, 10 K, and 15 K; the lack of saturation confirms the absence of ferromagnetic components. The slight curvature at 5 K is in agreement with the associated Brillouin function. The type of ordering cannot be extracted from bulk magnetic measurements. However, neutron-diffraction and muon spin relaxation measurements will help to determine the true magnetic ground state.

D. Neutron-diffraction experiments at low temperatures

Neutron-powder-diffraction experiments were carried out at 4 K and 40 K. The powder-diffraction patterns for 4 K and 40 K are identical as can be seen in Fig. 10. If the inflection point at 12 K in the magnetic susceptibility data were due to magnetic long-range order, the neutron powder patterns should show magnetic Bragg peaks at 4 K, or the intensities of the crystallographic peaks should change due to the magnetic contribution. However, no differences are found for these measurements, thus indicating that no magnetic long-range order is present down to 4 K as already expected from bulk magnetic data. Furthermore, the absence of broad features at 4 K suggests that no magnetic short-range order is present at this temperature. However, due to the weak magnetic moment of Re^{6+} ($S = 1/2$) and the fact that the sample resembles a fairly dilute magnetic system, potential broad features might be too weak to be observable.

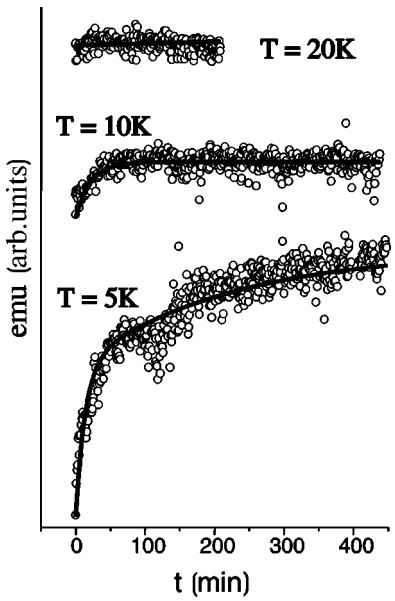

FIG. 8. Magnetic relaxation measurements at 5 K, 10 K, and 20 K using an external magnetic field of $H = 0.1$ T. The data sets acquired at 5 K and 10 K are fitted using a biexponential relaxation function. All three data sets are on the same scale using arbitrary offsets.

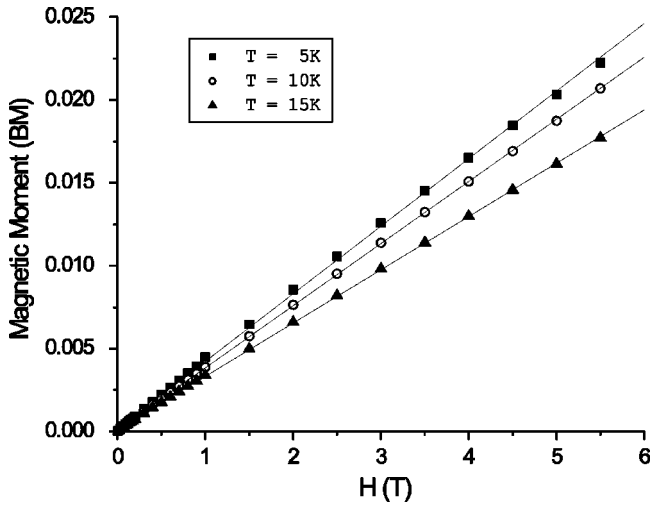

FIG. 9. Magnetization measurements at 5 K, 10 K, and 15 K, the solid lines are linear fits, only the 5 K data set deviates slightly from linear behavior (see text).

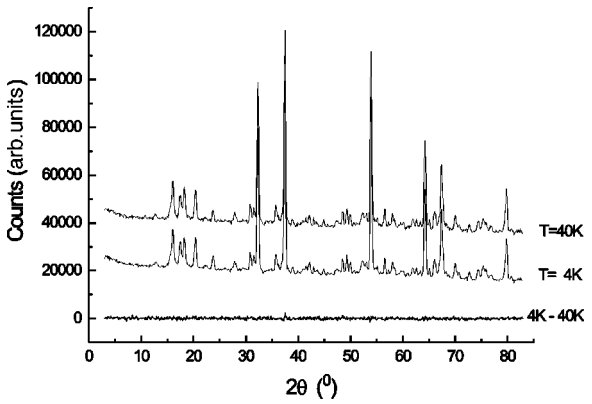

FIG. 10. Powder-neutron-diffraction data obtained at low temperatures. The data sets at 40 K and 4 K are identical, indicating that no magnetic long-range order is present in the sample. Data obtained on powder-diffraction instrument C2 at Chalk River.

E. Heat-capacity measurements

The heat-capacity data for the temperature range 0.5 K to 6 K are shown in Fig. 11. The measurement was carried out up to 30 K, but the data were unacceptably noisy above 6 K. However the data did not show any evidence of a lambda anomaly up to 30 K. The data for the temperature range 0.5 K to 6 K were fitted to Eq. (3.4)

$$C_p = \gamma T + \beta T^3, \tag{3.4}$$

where γT describes the electronic contribution and βT^3 the lattice contribution to the heat capacity. Since Li_4MgReO_6 is an insulator, as determined from two probe resistivity measurements, it is assumed that the electronic contribution to the heat capacity is entirely due to the inherent magnetism.

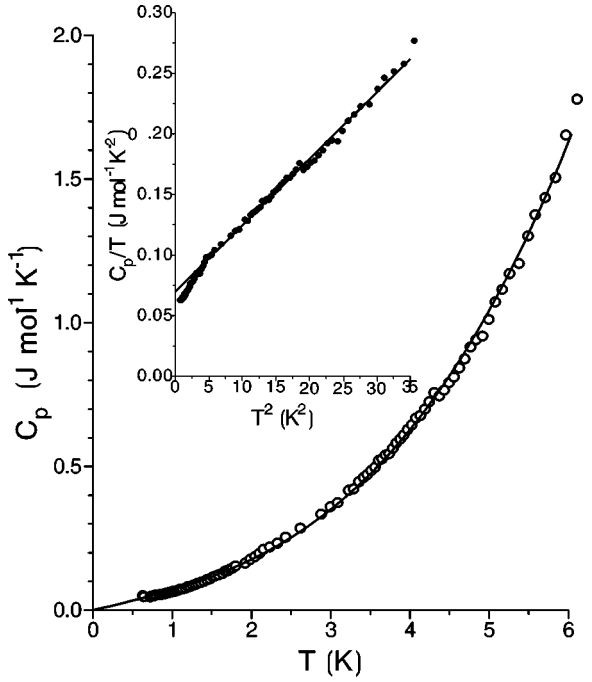

FIG. 11. Heat-capacity measurements at low temperatures. The solid line is the best fit for the function $C_p=\gamma T+\beta T^3$ (see text). The inset shows the same data and best fit plotted as C_p/T versus T^2.

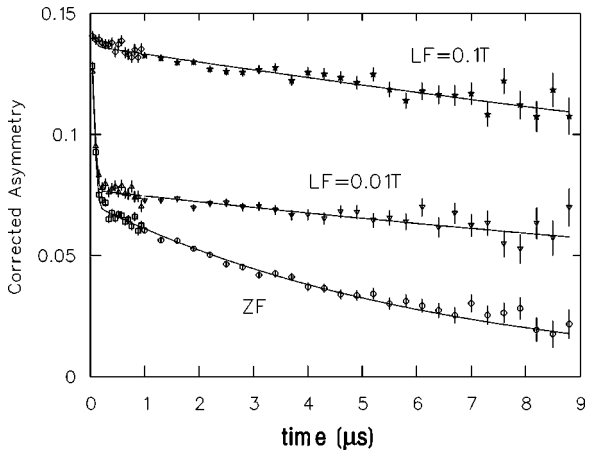

FIG. 12. Muon spin relaxation spectra for Li_4MgReO_6 as a function of a longitudinal magnetic field taken at 2.5 K. The zero-field and $H=0.01$ T data show pronounced relaxation during the first 200 ns, whereas the data collected with $H=0.1$ T lack this initial relaxation. The best fits according to Eq. (3.6) are shown as solid lines.

For spin glasses a linear temperature dependence of the magnetic heat capacity is expected.[19] The following coefficients are found for Li_4MgReO_6: $\gamma=0.070(2)$ J mol^{-1}K^{-2} and $\beta=0.0054(8)$ J mol^{-1}K^{-4}. The inset in Fig. 11 shows C_p/T versus T^2, which is linear as required according to Eq. (3.4), the slope represents β and the extrapolated ordinate intercept gives γ. The magnetic entropy S_m was obtained by extrapolating C_m/T to 0 K and to $T_f=12$ K and integrating over this temperature range according to Eq. (3.5).

$$S_m = \int_0^T \frac{C_m}{T'} dT'. \tag{3.5}$$

The total magnetic entropy is 0.84 J mol^{-1}K^{-1}. Whereas, the expected magnetic entropy is $R\ln(2)=5.76$ J mol^{-1}K^{-1}, thus the experimental magnetic entropy below T_f accounts for 14% of the expected entropy. This result is not unexpected, as it is well known for spin glasses that most of the magnetic entropy removal takes place above the glass transition temperature.[19]

F. Muon spin relaxation

The muon spin relaxation (μSR) experiments were carried out on the M13 surface μ^+ beamline at the TRIUMF facility, Vancouver, Canada. The zero-field (ZF) experiments were performed at temperatures between 125 K and 2.5 K. Additional measurements were carried out at 2.5 K in a longitudinal field (LF) of 0.01 T and 0.1 T. Several ZF/LF-μSR spectra collected at 2.5 K are shown in Fig. 12; clearly the relaxation behavior changes drastically upon increasing the longitudinal field strength. The two component form of the spin relaxation, along with the decoupling of the relaxation upon application of a longitudinal field are characteristic features of a (quasi)-static distribution of internal magnetic fields, such as would be present in a spin glass. In contrast, in zero applied field, long-range magnetic order antiferromagnetic or ferromagnetic would have resulted in a superimposed periodic signal due to muon spin precession. The ZF and $H=0.01$ T data show pronounced relaxation during the

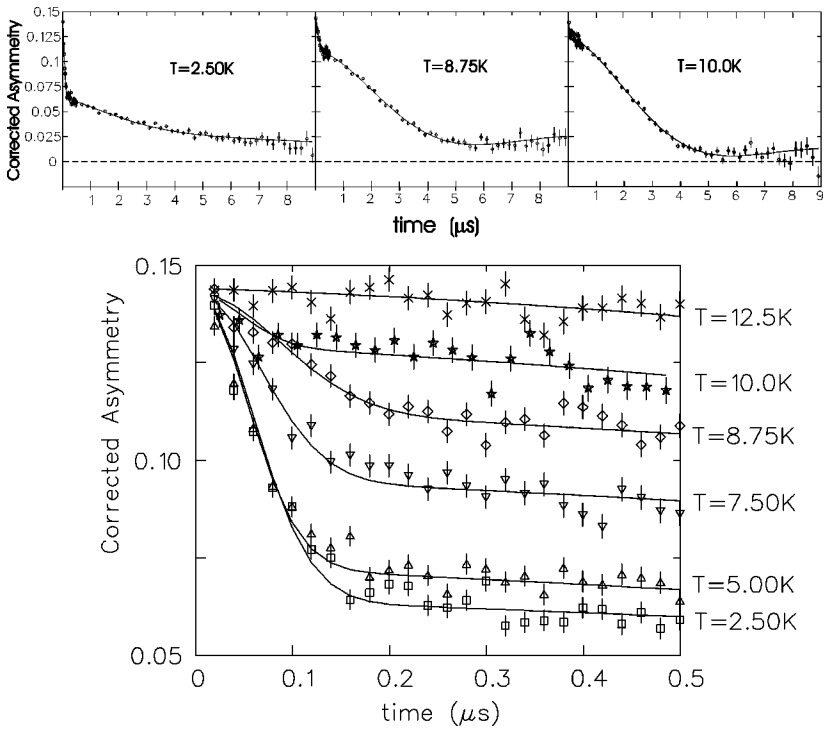

FIG. 13. Zero-field muon spin relaxation spectra for Li_4MgReO_6. The upper figures shows three different temperatures, 10 K, 8.75 K, and 2.50 K for the time intervals 0 to 10 μs. The graph at the bottom shows the details for the first 0.5 μs taken at six different temperatures, the solid lines are the best fits according to Eq. (3.6). Crosses = 12.5 K, stars = 10 K, diamonds = 8.75 K, down triangles = 7.50 K, up triangles = 5.00 K, and squares = 2.50 K.

first 200 ns. The data at longer times seem to flatten out with a fairly small negative slope for the 0.01 T experiment, which also indicates that the internal fields are essentially static. Upon increasing the longitudinal field strength to 0.1 T, the initial relaxation is decoupled leaving only weak relaxation due to remaining slow spin fluctuations, as expected in a cluster spin glass for $T \approx 0.2\ T_f$. ZF-μSR experiments were performed in the temperature range 2.5 K$<T<$125 K, these data show a marked temperature dependence (Fig. 13) for $T<12.5$ K, which is in agreement with the inflection point at 12 K for dc-magnetic susceptibility data reported earlier. The Gaussian relaxation is in agreement with the behavior expected for a dense distribution of (quasi)-static randomly oriented spins. This fact is in agreement with fully occupied Re^{6+} sites, in contrast to an exponential or square-root exponential behavior as expected for a dilute spin system. Furthermore, the increasing amplitude of the Gaussian relaxation function with decreasing temperature suggests a clustered spin glass, where the clusters grow in size as the temperature is lowered. The ZF data were fitted to a phenomenological fitting function (3.6), in which the relaxation without the typical (Kubo-Toyabe) 1/3 recovery was resembled using the following fitting function.

$$Asym_{cor} = A[(1-O_{frac})\exp(-\Delta^2 t^2)\exp(-\lambda_s t)] + A\left[O_{frac}\frac{2}{3}\exp(-\sigma_f^2 t^2) + O_{frac}\frac{1}{3}\exp(-\lambda_t t)\right], \tag{3.6}$$

where t is equal to time in μs and A is the asymmetry of the counter that accounts for the efficiencies of the forward and backward counters and the properties of muon decay. $Asym_{cor}$ is the corrected asymmetry and O_{frac} denotes the volume fraction of frozen spins; Δ, λ_s, σ_f, and λ_t are inverse relaxation times. The first bracket in Eq. (3.6) describes the nonordered fraction of the sample, where the source of relaxation is nuclear dipolar fields. This is mainly described by the Gaussian function, however, an exponential term was multiplied in order to improve the fit. The exponential function could reflect the possible existence of multiple muon sites, which explains the deviation from a truly Gaussian relaxation function, in contrast to a single muon site. The parameters Δ and λ_s are temperature independent and were determined from fits at 125 K, these parameters were held fixed for the low-temperature fits. The second bracket in Eq.

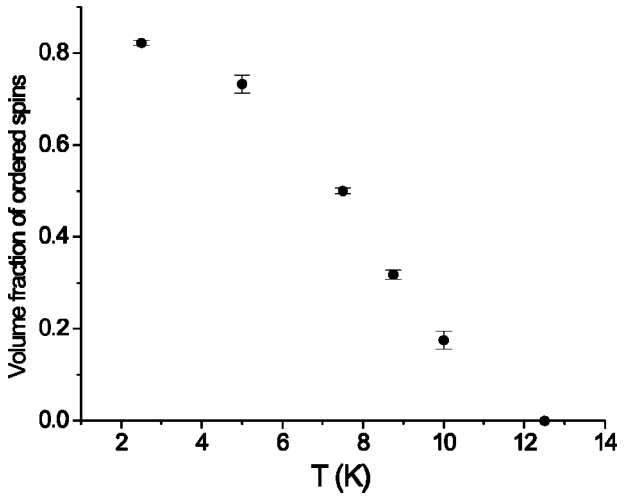

FIG. 14. Volume fraction of frozen spins as a function of temperature as derived from muon spin-relaxation measurements.

(3.5) describes the volume [fraction of frozen spins (fraction of (quasi)-static electronic spins] using a Gaussian type function with a characteristic inverse relaxation time σ_f and an exponential term with parameter λ_t for the 1/3 tail in the ordered state. For the temperature range 2.5 K$\leqslant T \leqslant$10 K the inverse relaxation times σ_f were found to be in the range 10 to 13 μs^{-1}. Using Eq. (3.7)

$$B_{local}=\frac{\sigma_f}{\gamma_\mu} \tag{3.7}$$

and the value $\gamma_\mu=861.5$ Mrad s^{-1} T^{-1} for the gyromagnetic ratio for a muon, we obtain an averaged characteristic internal magnetic field of approximately 0.014 T. The size of the field indicates that the Re^{6+} electronic moments must be the source of the internal field as any nuclear dipolar fields would be much smaller and temperature independent. The observed characteristic local field is in agreement with the fact that the muon spin relaxation is completely decoupled upon application of an external longitudinal field of 0.1 T, whereas the smaller longitudinal field of 0.01 T was not able to significantly decouple the relaxation (except for that due to nuclear dipolar fields in the nonordered volume fraction). The freezing of the magnetic moments at low temperatures clearly indicates that the ground state of Li_4MgReO_6 is best described as a spin-glass and not as a spin-liquid state. For each temperature the volume fraction of frozen spins O_{frac} was determined from the fits of function (3.6); these results are shown in Fig. 14. The gradual increase of the ordered fraction below 12 K allows the conclusion that the spin-glass freezing consists of an island growth process. The volume fraction of frozen spins levels off slightly above 0.8, however, due to systematic errors, the true value might be closer to 1.0 (for example in underestimating the fraction of muons landing in the sample holder). The sample is considered to be completely frozen at 2.5 K.

IV. CONCLUSIONS

The crystallographic and magnetic properties of Li_4MgReO_6 were investigated. Li_4MgReO_6 crystallizes in space group $C2/m$, having a three-dimensional network of Re^{6+} ions. The Re^{6+} sublattice is best described as a distorted face sharing tetrahedral framework. Magnetic bulk measurements show hysteresis behavior below 12 K, thus indicating possible cooperative magnetism at low temperature. From low-temperature powder-neutron-diffraction experiments, magnetic long-range order can be ruled out for Li_4MgReO_6. μSR experiments clearly indicate a spin-glass ground state, where the spin freezing process is completed at approximately 2.5 K. We found an averaged characteristic internal magnetic field of approximately 0.014 T. Heat-capacity measurements show that most of the entropy removal occurs above T_f, thus supporting the finding of a spin-glass ground state. The spin-glass ground state is attributed to the high degree of geometric magnetic frustration inherent on the Re^{6+} sublattice. Furthermore, bonding disorder due to Mg, Li disorder favors the spin-glass ground state. Each magnetic exchange path is complicated and involves in total five ions, a simple model based on superexchange cannot describe the magnetic interactions.

ACKNOWLEDGMENTS

This work has benefitted from the use of the Intense Pulsed Neutron Source at Argonne National Laboratory that is funded by the U.S. Department of Energy, BES-Materials Science, under Contract No. W-31-109-ENG-38. We would like to thank Simine Short for collecting the powder-neutron-diffraction data at IPNS. We also acknowledge the support of Ian Swainson and the beam time on the powder neutron diffractometer C2 in Chalk River, which is operated by NPMR and NRC, Canada. We appreciate the hospitality of the TRIUMF μSR user facility. Furthermore, we would like to acknowledge Andrew Wills for his support with the neutron powder refinements and valuable discussions. Our thanks extend to N. P. Raju for help with the heat-capacity measurements. Financial support from the Natural Science and Engineering Research Council of Canada (NSERC, J.E.G.) is gratefully acknowledged. G.M.L. is thankful to the CIAR superconductivity program and NSERC.

[1] W.C. Koehler, E.O. Wollan, H.L. Yakel, and J.W. Cable, Phys. Lett. **9**, 93 (1964).
[2] M. Bieringer and J.E. Greedan, J. Solid State Chem. **143**, 132 (1999).
[3] B.D. Gaulin and M.F. Collins, Can. J. Phys. **62**, 1132 (1984).
[4] B.D. Gaulin and M. Collins, J. Phys. C **19**, 5483 (1986).
[5] K. Hirakawa and H. Ikeda, in *Magnetic Properties of Layered Transition Metal Compounds*, edited by L.J. de Jongh (Kluwer Academic, Boston, 1990).
[6] P.W. Anderson, Mater. Res. Bull. **8**, 153 (1973).
[7] P. Fazekas and P.W. Anderson, Philos. Mag. **30**, 423 (1974).
[8] K. Hirota, Y. Nakazawa, and M. Ishikawa, J. Phys.: Condens. Matter **3**, 4721 (1991).
[9] S.J. Clarke, A.J. Fowdes, A. Harrison, R.M. Ibberson, and M.J. Rosseinsky, Chem. Mater. **10**, 372 (1998).
[10] Y.J. Uemura, A. Keren, K. Kojima, L.P. Le, G.M. Luke, W.D. Wu, Y. Ajiro, T. Asano, Y. Kuriyama, M. Mekata, and H. Kikuchi, Phys. Rev. Lett. **73**, 3306 (1994).
[11] A.S. Wills and A. Harrison, J. Chem. Soc., Faraday Trans. **92**, 2161 (1996).
[12] J.N. Reimers, J.E. Greedan, and M. Sato, J. Solid State Chem. **72**, 390 (1988).
[13] R. Scholder, K.L. Huppert, and P.P. Pfeiffer, Angew. Chem. Int. Ed. Engl. **2**, 375 (1963).
[14] G. Lang, Z. Anorg. Allg. Chem. **348**, 246 (1966).
[15] A. Ferretti, D.B. Rogers, and J.B. Goodenough, J. Phys. Chem. Solids **26**, 2007 (1965).
[16] T. Betz and R. Hoppe, Z. Anorg. Allg. Chem. **512**, 19 (1984).
[17] A.C. Larson and R.B. von Dreele, GSAS, *General Structure Analysis System*, LANSCE, Los Alamos National Laboratory, Los Alamos, 1994.
[18] A.C. Porte, *Transition-Metal Ions-Electron Spin Resonance* (Alden Press, Oxford, 1979).
[19] J.A. Mydosh, *Spin Glasses, An Experimental Introduction* (Taylor & Francis, London, 1993).